The following article appeared in Environmental Technology & Innovation Volume 28, November 2022, 102878 and may be found at: https://doi.org/10.1016/j.eti.2022.102878

Environmental Technology & Innovation 28 (2022) 102878

Contents lists available at ScienceDirect

Environmental Technology & Innovation

journal homepage: www.elsevier.com/locate/eti

Autotrophic denitrification of nitrate rich wastewater in fluidized bed reactors using pyrite and elemental sulfur as electron donors

Maria F. Carboni [a,*], Simon Mills [a], Sonia Arriaga [a,b], Gavin Collins [c,d], Umer Z. Ijaz [d], Piet N.L. Lens [a]

[a] National University of Ireland Galway, H91 TK33, Galway, Ireland
[b] División de Ciencias Ambientales, Instituto Potosino de Investigación Científica y Tecnológica, Camino a la Presa San José 2055, Lomas 4a Sección, 78216, San Luis Potosí, CP, Mexico
[c] School of Chemical and Biological Sciences, and Ryan Institute, National University of Ireland Galway, University Road, Galway H91 TK33, Ireland
[d] Water and Environment Group, School of Engineering, University of Glasgow, Glasgow G12 8LT, United Kingdom

ARTICLE INFO

Article history:
Received 26 June 2022
Received in revised form 1 August 2022
Accepted 13 August 2022
Available online 23 August 2022

Keywords:
Pyrite
Elemental sulfur
Fluidized bed rector
Nitrogen removal
16S rRNA
Community assembly

ABSTRACT

This study compared denitrification performances and microbial communities in fluidized bed reactors (FBRs) carrying out autotrophic denitrification using elemental sulfur (S^0) and pyrite (FeS_2) as electron donors. The reactors were operated for 220 days with nitrate loading rates varying between 23 and 200 mg N-NO_3^-/L·d and HRT between 48 and 4 h. The highest denitrification rates achieved were 142.2 and 184.4 mg N-NO_3^-/L·d in pyrite and sulfur FBRs, respectively. Pyrite-driven denitrification produced less SO_4^{2-} and no buffer addition was needed to regulate the pH. The sulfur FBR needed instead $CaCO_3$ to maintain the pH neutral and consequentially more sludge was produced ($CaSO_4$ precipitation). The active community of pyrite-based systems was investigated and *Azospira sp.*, *Ferruginibacter sp.*, *Rhodococcus sp.* and *Pseudomonas sp.* were the predominant genera, while *Thiobacillus sp.* and *Sulfurovum sp.* dominated the active community in the sulfur FBR. However, *Thiobacillus sp.* became more dominant when operating at elevated nitrogen loading rate. Patterns of diversity and microbial community assembly were assessed and revealed three distinct stages of microbial community succession which corresponded with the operation of a period of high influent nitrate concentration (135 mg N-NO_3^-/L). It is proposed that a high degree of functional redundancy in the initial microbial communities may have helped both reactors to respond better to such high influent nitrate concentration.

1. Introduction

Nitrogen contamination in waterbodies is a major environmental concern as it can lead to eutrophication and algal blooms. The presence of nitrate and/or nitrite in drinking water can also cause methemoglobinemia and carcinogenic diseases (Jessen et al., 2017; Zhang et al., 2020). Wastewaters with high (greater than 1000 mg N-NO_3^-/L) nitrate

* Correspondence to: Department of Microbiology, School of Natural Sciences and Ryan Institute, National University of Ireland Galway, H91 TK33, Galway, Ireland.
E-mail address: m.carboni2@nuigalway.ie (M.F. Carboni).

https://doi.org/10.1016/j.eti.2022.102878

concentrations originate from several industries, including fertilizer and explosives production, metals finishing and the nuclear industry (Liao et al., 2013; Fernández-Nava and Soons, 2010).

Conventionally, nitrate and nitrite removal is carried out by heterotrophic bacteria. However, the heterotrophic denitrification process is disadvantageous for wastewaters with low C/N ratio, since external organic carbon must be added, which increases costs and may lead to organic contamination at the end of the process. The application of autotrophic denitrification for wastewaters with low organic carbon content is an attractive alternative (Li et al., 2020; Lu et al., 2011; Sahinkaya et al., 2014). The most common electron donors for autotrophic denitrification are reduced sulfur compounds (RSCs) (Khanongnuch et al., 2019; Ucar et al., 2020; Zou et al., 2016) or hydrogen (Rezania et al., 2005; Vasiliadou et al., 2009). Elemental sulfur is the RSC most applied in autotrophic denitrification, but it has some disadvantages that make the process more costly. Significant base addition is required (4.57 g $CaCO_3$/g NO_3^-) to maintain the optimal pH for sulfur oxidizing bacteria (between 6 and 7). In addition, high levels of sulfate are produced (2,51 g SO_4^{2-}/g NO_3^-). Iron sulfide minerals (e.g. pyrite, pyrrhotite and marcasite) have recently attracted attention as sustainable substrates for autotrophic denitrifying bacteria (Hu et al., 2020; Pu et al., 2015), they are cheap, ubiquitous in the earth's crust (Ogbughalu et al., 2020) and are stable, with low solubility in anoxic environments. This behavior makes them suitable, slow-release electron donors for autotrophic denitrification. Preliminary experiments with pyrite showed several advantages such as the preservation of a stable pH without the addition of any base addition (Hu et al., 2020) and low sulfate production (Di Capua et al., 2020; Carboni et al., 2021), however its application might lead to lower nitrogen removal rates compared with S^0-driven denitrification (Liu et al., 2021). Therefore, further studies on pyrite-driven autotrophic denitrification are of great interest, mainly aiming at increasing denitrification rates in continuous-flow bioreactors.

In previous research no systematic study has been carried out that comparatively investigated the differences and evaluated the advantages and drawbacks of the two electron donors (pyrite and elemental sulfur). The present study explored the performance of two fluidized bed reactors (FBRs) with either pyrite (FeS_2) or elemental sulfur (S^0) as electron donor for which autotrophic denitrification occurs according to the following reactions (Carboni et al., 2021):

$$FeS_2 + 3NO_3^- + 2H_2O \rightarrow Fe(OH)_3 + 1.5N_2 + 2SO_4^{2-} + H^+ \quad (1)$$

$$5S^0 + 6NO_3^- + 2H_2O \rightarrow 5SO_4^{2-} + 3N_2 + 4H^+ \quad (2)$$

FBRs for autotrophic denitrification have not been extensively investigated in S^0 systems and were never investigated in combination with FeS_2. Therefore, this configuration has been chosen in the current study to improve the solubilization of sulfur and pyrite particles and to explore the possible enhancement of denitrification rates. Moreover, for the first time, the active microbial community of pyrite-based systems was investigated.

The two reactors were operated in parallel, under the same operational conditions, in order to evaluate, in every phase, the differences between the two RSCs. The specific objectives of this study were: (i) to compare the denitrification performances of pyrite and sulfur as electron donors in FBRs; (ii) to investigate the robustness of the two systems by decreasing the HRT and varying the nitrate concentration; and (iii) to analyze the microbial community dynamics of the total and active microbial communities in each reactor.

2. Materials and methods

2.1. Source of biomass and media composition

Sulfur (SR) and pyrite (PR) fluidized bed reactors were respectively inoculated with sulfur and pyrite oxidizing denitrifying cultures, which were enriched as described previously (Carboni et al., 2021). Sterile anoxic basal medium used during the enrichment process was prepared as described by Stams et al. (1993) comprising of (g/L): 1.2 KNO_3; 0.41 KH_2PO_4; 0.53 $Na_2HPO_4{\cdot}2H_2O$; 0.3 NH_4Cl; 0.3 NaCl; 0.1 $MgCl_2{\cdot}6H_2O$; 0.11 $CaCl_2{\cdot}2H_2O$ and 4 $NaHCO_3$. 0.2 mL/L vitamin solution 1 mL/L acid and alkaline trace elements solution; 0.1 g/L yeast extract (Alfa Aesar, Ward Hill, USA) and 1 mL/L resazurin sodium salt solution (Fischer scientific, Hampton, USA) were also added to the medium. The enriched cultures were stored at 4 °C prior their use in the reactors.

2.2. Bioreactor set up

The selected enrichments were used to inoculate two glass FBRs (30%, v/v) of 1020 mL with 800 mL working-volume and 220 mL headspace (Fig. S1). Anoxic conditions were provided immediately after inoculation by flushing N_2 into the reactors for 30 min. The FBRs were maintained at 30 °C with a thermostatic recirculation bath. 125 g FeS_2 (99+% grade, 0.15–0.48 cm diameter, from Fischer Scientific, Hampton, USA) and 75 g of chemically synthesized S^0 (99.5% grade, 150 μm diameter, from Fischer Scientific, Hampton, USA) mixed with 75 g $CaCO_3$(98+% grade, from Fischer Scientific, Hampton, USA) were added to the FBRs as electron donors with static bed depths of approximately 10 cm. The liquid phase inside the reactor was continuously recirculated in upflow mode by a peristaltic pump (Masterflex Cole-Parmer, Chicago, USA) at flow rate of 200 mL/min allowing a bed expansion of 30%–40% in both FBRs.

Table 1
Operational conditions of the FBRs during the study.

Phase	*Time* [d]	*HRT* [h]	C_o [mg N-NO_3^-/l]	*NLR* [mg N-NO_3^-/l d]
I (batch mode)	0–22	–		–
II	22–43	48	45	23 (±2.9)
III	43–57	24	45	47.4 (±4.6)
IV	58–70	18	45	59.7 (±2.5)
V	70–84	12	45	90 (±1.2)
VI	84–121	24	135	132.43 (±6.4)
VII	120–146	8	45	132.6 (±3.7)
VIII	146–161	6	35	133.9 (±2.9)
IX	161–220	4	35	200.4 (±4.5)

2.3. FBR start-up and operation

The FBRs were operated in fed-batch mode for the first 22 days to facilitate bacterial attachment to the electron donor particles. 400 mL of the medium was replaced with fresh medium four times during phase I. From day 22 on, the reactors were operated in continuous mode, under 8 different operational phases (II–IX, Table 1). The reactors were fed with the same synthetic medium used during the enrichment but without resazurin solution, the yeast extract was not provided anymore from phase III (day 43) onward and nitrate concentrations varied during the different phases (Table 1). The influent pH was between 6.9 and 7.5. The HRT varied between 48 and 4 h (Table 1). From phase II to phase V a decrease in the HRT and a consequential increase in the nitrate loading rate (NLR) was applied (Table 1). In phase VI, to investigate the process' response to highly polluted wastewaters the influent nitrate concentration of the synthetic medium was increased from 45 to 135 mg N-NO_3^-/L and the HRT was increased from 12 to 24 h. Afterwards, in phase VII and VIII the NLR was constant but the nitrate concentration in the influent was gradually decreased to 45 mg N-NO_3^-/L in phase VI and 35 mg N-NO_3^-/L in phase VIII and XI. Simultaneously, the HRT was decreased from 8 to 4 h in phase VII–XI.On day 186, 25 g of pyrite and sulfur particles were added to the FBRs to understand if the decrease in the denitrification efficiency of the last phase was related to limited availability of electron donors. Phase IX was divided in IX-A and IX-B to distinguish before and after the addition of pyrite/sulfur in the FBRs.

Liquid samples were collected daily while gas samples were collected at the end of every phase for N_2O measurement. Solid samples were collected on day 162 and at the end of the trial (day 220). Samples for microbial community analysis were collected before every change in the HRT from the bottom of the reactors.

2.4. DNA/RNA extraction, cDNA synthesis and PCR

Samples for microbial community analysis (2 mL) were collected in triplicate on days 0, 82, 121, 162 and 220. In addition, triplicate biofilm samples were collected from the FBR walls on day 220. All samples were stored at −80 °C after snap-freezing in liquid nitrogen. Cells were lysed by incubating with proteinase K at room temperature for 10 min, followed by mechanical disruption by bead beating in RLT buffer (QIAGEN, Hilden, Germany). DNA and RNA were co-extracted using a phenol–chloroform co-extraction according to the protocol described by (Griffiths et al., 2000).

RNA extracts were DNase treated with the QuantiTect Rev. Transcription Kit (QIAGEN, Hilden, Germany) following the manufacturer's instructions. Complete removal of contaminating DNA was confirmed by polymerase chain reaction (PCR) with the 515F 806R primer pair (Parada et al., 2016). Subsequently, synthesis of cDNA from RNA was performed using the QuantiTect Rev. Transcription Kit (QIAGEN, Hilden, Germany) according to the manufacturer's instruction.

PCR amplification of DNA and cDNA was performed using the 515F 806R primer pair (Parada et al., 2016). The amplification program consisted of an initial denaturation step at 94 °C for 3 min, 35 cycles of denaturation at 94 °C for 45 s, annealing at 50 °C for 1 min, extension at 72 °C for 90 s, and a final extension at 72 °C for 10 min using Platinum™ II Hot-Start PCR Master Mix (2×) reagents from Invitrogen (Carlsbad, USA). The PCR products were checked in 1% agarose gel electrophoresis. Library preparation and sequencing was carried out by Novogene (Cambridge, UK) on the NovaSeq 6000 platform.

2.5. Bioinformatic analysis

Amplicon Sequencing Variants (ASVs) were constructed using Qiime2 workflow according to Trego et al. (2021). All code for sequence processing can be found at (https://github.com/umerijaz/tutorials/blob/master/qiime2_tutorial.md). In the final analysis, 8838 clean ASVs were extracted for n = 72 samples on which different multivariate statistical analyses were performed using R software. Alpha diversity, beta diversity and differential heat tree analysis were conducted as described previously (Mills et al., 2021). Other statistical analysis, including the R packages used are described in detail in the Supplementary material.

Table 2
Nitrate removal efficiency (%) and denitrification rates (mg N-NO_3^-/L d) in the FBRs achieved in the different phases.

Phase	*HRT* [h]	C_o[mg N-NO_3^-/l]	*Removal efficiency [%]*		*Denitrification rate* [mg N-NO_3^-/ l d]	
			P_Reactor	*S_Reactor*	*P_Reactor*	*S_Reactor*
II	48	45	78.9 ± 33.7	84.5 ± 29.7	17.8 ± 7.8	19.2 ± 7.1
III	24	45	97.1 ± 8.3	100	45.3 ± 6.1	46.6 ± 3.9
IV	18	45	94.3 ± 0.9	95.9 ± 1.5	56.1 ± 2.2	57.1 ± 2.7
V	12	45	95.2 ± 2.1	95.8 ± 1.7	86.5 ± 2.6	87.2 ± 3.5
VI	24	135	69.3 ± 16.8	93.9 ± 6.2	92.2 ± 25.2	124.4 ± 9.8
VII	8	45	73.1 ± 5.7	90.9 ± 4.1	96.7 ± 7.7	119.9 ± 6.6
VIII	6	35	89.9 ± 9.7	87.7 ± 5.2	120.3 ± 12.5	117.6 ± 8.8
IX-A[a]	4	35	70.9 ± 10.7	61.7 ± 11.3	142.4 ± 22.2	124.1 ± 22.7
IX-B[b]	4	35	60.9 ± 9.3	91.2 ± 6.3	122.56 ± 18.7	184.2 ± 12.8

[a]Days 146–186: before the addition of pyrite and elemental sulfur.
[b]Days 186–220: after the addition of pyrite and elemental sulfur.

2.6. Analytical methods

Liquid samples were filtered through a 0.22 μm membrane filter. Nitrite, nitrate and sulfate concentrations were determined by ion chromatography (ThermoFisher Scientific, Waltham, USA) with an IonPac AS14 A 4 × 250 mm column coupled with an AG14 A 4 × 50 mm guard column and sodium carbonate 3.03 mM/sodium bicarbonate 0.97 mM eluent at a flow rate of 1 mL/min (Florentino et al., 2020). NH_4^+ and Fe^{2+} concentrations were determined using a Gallery+ analyzer (Thermo Scientific) following the manufacturer's protocols. Total organic carbon (TOC) measurements were carried out using a TOC analyzer (TOC-L, Shimadzu, Kyoto, Japan). Sulfide concentrations were determined spectrophotometrically using methylene blue as previously described by Cline (1969) with a Shimadzu UV-1900 spectrophotometer (Shimadzu, Kyoto, Japan). pH was measured using a Mettler Toledo FiveEasy™ (FP20, US) pH-meter. N_2O was measured with a gas chromatograph (7890B, Agilent, Santa Clara, USA), equipped with a flame induction detector (FID) heated at 250 °C. Helium was used as the carrier gas with a flow rate of 2.5 mL/min. The infrared absorption spectra of the solid precipitate withdrawn from the reactors were examined by a Fourier transform infrared attenuated total reflectance (FTIR-ATR) spectrophotometer (ATR-Nicolet iS5, Thermo scientific) in the range from 4000 to 525 cm^{-1} with a 4 cm^{-1} resolution. Total Fe analyses were performed with an ICP-OES (ThermoFisher, Scientific Walthan, USA) operated at RF power: 1.2 kW, argon plasma flow rate: 12 L/min, auxiliary argon flow rate: 1 L/min and nebulizer argon flow rate: 0.7 L/min. Iron was read on radial mode at 238.204 nm (Costa et al., 2020). Total solids (TS), volatile solids (VS), and fixed solids of the material collected from the FBRs at the end of the trials were measured according to the APHA procedures (APHA, 2012).

3. Results

3.1. Effect of HRT and influent nitrate concentration

From phase II to V, the nitrate concentration of the effluent from both reactors was generally below 3 mg N-NO_3^-/L (Fig. 1), resulting in 95%–100% denitrification efficiency (Table 2) and no nitrite accumulation (Fig. 1B). From day 82 in phase VI, the behavior of the two FBRs differed as a result of the high influent nitrate concentration. Denitrification activity decreased in SR until day 93 when the effluent nitrate concentration was 33.01 mg N-NO_3^-/L. Subsequently, after the first 11 days of phase VI, de nitrate effluent concentration decreased to approximately 3.65 mg N-NO_3^-/L between days 102 and 121. In PR, the denitrification activity during phase VI decreased, resulting in an average nitrate concentration in the effluent of 177.77 mg N-NO_3^-/L (nitrate removal efficiency of 70% - Table 2). In phase VI, nitrite accumulated in both reactors. Similar to nitrate in SR, nitrite reached a peak of 8.55 mg N-NO_2^-/L on day 93 and decreased below the detection limit from day 102 to 121. In contrast, in PR nitrite accumulated for all of phase VI reaching a maximum concentration of 24.86 mg N-NO_2^-/L on day 91. In phase VII, the two reactors followed the same trend observed in phase VI, with an average denitrification efficiency of 73.11% and 90.93% in PR and SR, respectively. In phase VIII (influent concentration 35 mg N-NO_3^-/L and HRT 6 h), PR performed better than SR, reaching average effluent nitrate concentrations of 0.85 and 3.34 mg N-NO_3^-/L, respectively, corresponding to a denitrification removal efficiencies of 90% and 88%; and denitrification rates of 120.3 mg N-NO_3^-/L·d and 117.6 mg N-NO_3^-/L·d in PR and SR, respectively (Table 2).

In phase IX, the NLR was increased from 133.9 to 200 mg N-NO_3^-/L·d and the denitrification efficiency decreased in both reactors. From days 162 to 186, PR had higher nitrate removal efficiencies (71%) than SR (62%). After the addition of sulfur on day 186 the denitrification efficiency of SR reached 92.5% and achieved its maximum denitrification rate of 186.8 mg N-NO_3^-/L·d. However, when new pyrite particles were added on day 186, the denitrification efficiency of PR did not improve. Effluent nitrite concentrations from phase VII to IX were always below 6 mg N-NO_2^-/L in both reactors.

The pH and the TOC (Fig. S2) in SR stayed between 6.5–7.4 and <30 mg/L, respectively. PR, on the hand, had an accumulation of TOC in phase II, up to 280 mg/L and a concomitant pH drop from 7 to 5.5. From phase III, the TOC decreased to a concentration always below 15 mg/L and the pH was stable in the neutral zone.

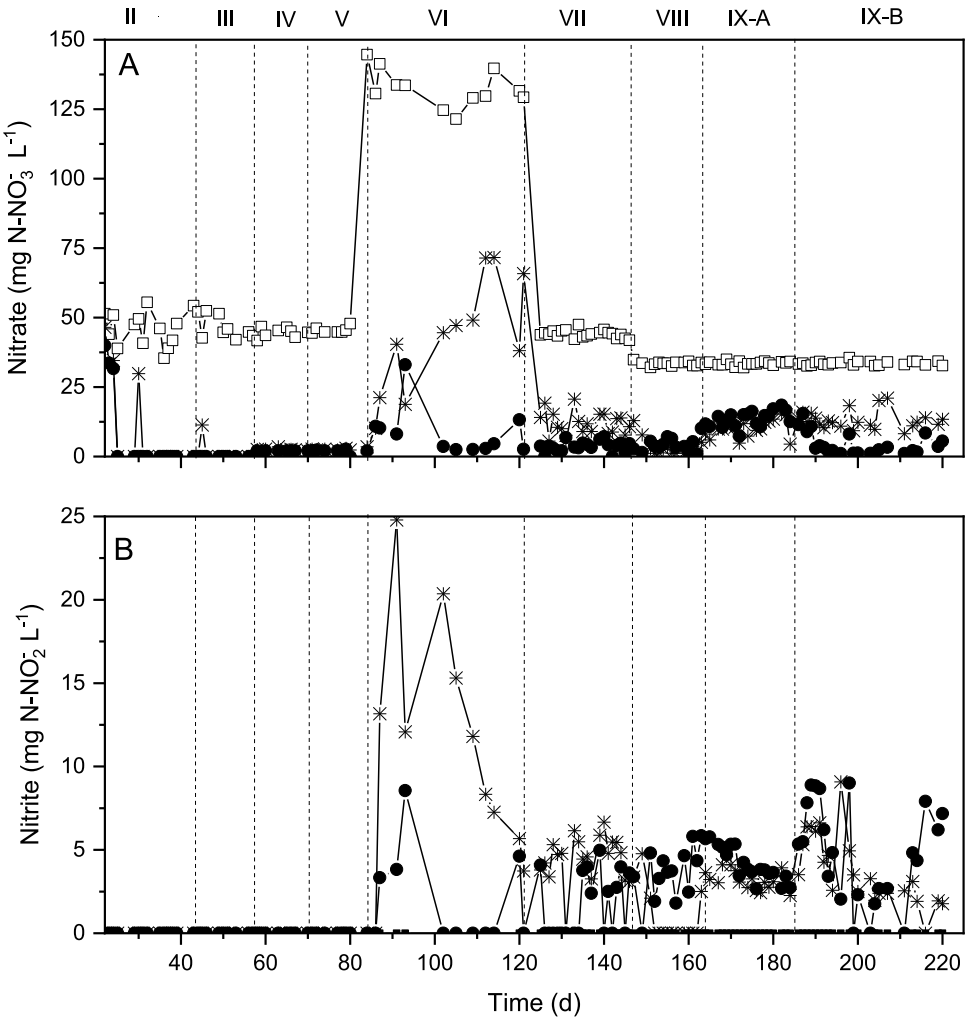

Fig. 1. Nitrate (A) and nitrite (B) concentrations in pyrite reactor effluent (*), sulfur reactor effluent (•) and in the influent (□) at the different conditions tested.

3.2. Sulfate production

In both reactors, the measured sulfate concentrations in the effluent values were lower than the theoretical values expected from stoichiometry (Eqs. (1) and (2)) (Fig. 2). Particularly, sulfate concentrations were often below the detection limit in PR's effluent. In Table S.1 the sulfate measured in the two reactor effluents is expressed as percentage of the theoretical values expected from the stoichiometry in every phase. For PR, extremely low sulfate concentrations were produced with values always below 4.13% of the theoretical expected concentration. In SR in phase IX-B (after the addition of sulfur particles) there was an increase in the sulfate concentration from an average 17.36% in phases between III and IX-A to 71.22% in phase IX-B (Table S1).

A peak at 800–1200 cm^{-1} was detected by FTIR-ATR analyses (Fig. S3) of solid samples from both reactors, which is typical of sulfate minerals like ammonium, sodium or calcium sulfate (Kadam et al., 2010; Kiefer et al., 2018). Since ammonium and sodium were introduced with the medium while calcium was present in SR because of the addition of $CaCO_3$, these results indicate that some sulfate precipitation occurred due to the binding of SO_4^{2-} with cations. Moreover a peak between 2700–3700 cm^{-1} was detected in the pyrite samples (Fig. S3), which is typical of iron sulfate precipitation (Di Capua et al., 2020; Majzlan et al., 2011).

The total and ferrous iron concentrations measured in PR effluent were below 1 mg/L as expected from the stoichiometry. Thus, in the pyrite reaction (Eq. (1)) the ferric iron bound with hydroxides and precipitates. This was also confirmed by FTIR-ATR (Fig. S3), where the peaks between 1600–1400 cm^{-1} are characteristic of $Fe(OH)_3/Fe(OH)_2$ (Wang et al., 2011).

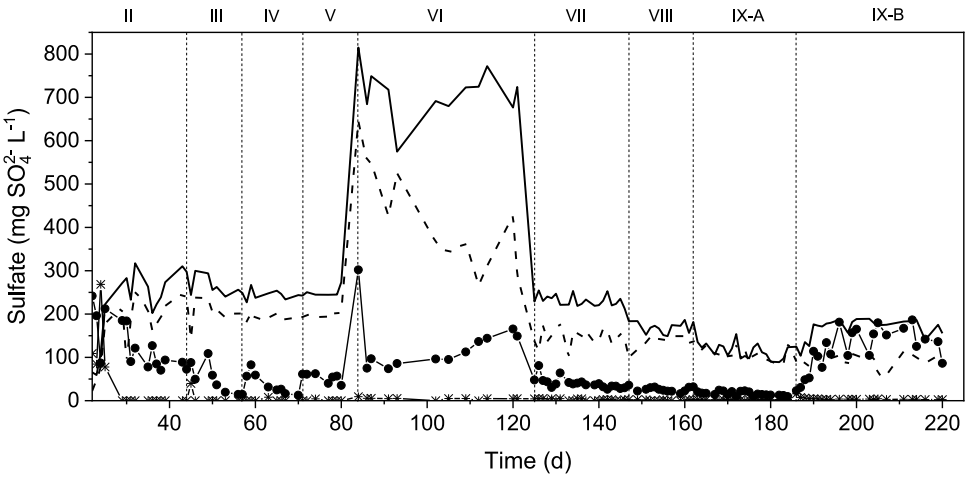

Fig. 2. Sulfate concentration in PR (*) and SR effluents (•) and theoretical sulfate expected from the amount of nitrate reduced in SR (—) lines and PR (- - -).

3.3. Microbial community evolution

3.3.1. Microbial community richness and diversity

Alpha diversity analysis revealed similar behavior in SR and PR for both the active (cDNA) and total (DNA) communities (Fig. A & B). Three distinct stages of microbial community succession were identified in the total community of both systems (Fig. 3A & B). High levels of richness, evenness and diversity characterized the first stage (days 0 and 82). All alpha diversity indices decreased during the second stage (days 121 and 163), following the high influent NO_3^- concentration period. Alpha diversity increased again in the final stage (day 220), reaching levels like that of the first stage. Shannon diversity decreased over time in the active community from day 0 to day 220. Evenness also decreased linearly over time in the active community, whereas species richness remained more stable. Similar successional patterns in beta diversity of the total and active communities were identified (Fig. 3C–F). Three different clusters were distinguishable, grouped on days 0 and 82, days 121 and 162 and day 220 (suspended and attached biomass). SR and PR total and active communities clustered separately (Fig. 3G) and electron donor explained approximately 35% of the total variability according to PERMANOVA ($p = 0.001$). In addition, the active community in both cases clustered within the total community.

3.3.2. Taxonomic diversity

Thiobacillus and *Sulfurovum sp*. dominated the SR total community (Fig. S4). *Thiobacillus sp.* relative abundance (RA) increased from around 30% on day 82 to approximately 75% on day 162 following the high influent NO_3^- concentration period (Phase VI). On day 220, after the final NLR increment, *Thiobacillus sp.* RA decreased while *Sulvurovum*, *Pseudomonas* and *Parvibaculum sp.* were the most relatively abundant genera. In the active community, *Thiobacillus* contributed only around 5% RA on days 0 and 82, while the most active taxa were *Sulfurovum, Pseudomonas* and *Parvibaculum*. On day 220, *Sulfurovum sp.* dominated the active community with a RA higher than 50% (Fig. S4).

The community present in PR was more mixed on days 0 and 82, while the genera *PHOS-HE36* and *1013-28-CG33* belonging to *Ignavibacteria* and *Gammaproteobacteria* classes, respectively, dominated on days 121 and 162. Day 220 was dominated by *Pseudomonas*, *Lentimicrobium*, *Petrimonas* and *Azospira*. The taxonomic composition varied in three stages similarly to alpha and beta diversity. *Pseudomonas* was dominant in the active community, on days 0 and 82 but its RA decreased to around 5% in the other time points. On day 220 the most dominant active bacteria were *Azospira* (RA 25%), *Syntrophomonas* (RA 20%) and *Petrimonas* (RA 5%). Fig. 4 compares the most abundant taxa in the total and active communities. Comparing SR and PR active communities it is clear that the classes *Ignavibacteria*, *Gammaproteobacteria* and *Bacteriodota* (*Lentimicrobium*) are characteristic of the pyrite-driven denitrification, while the *Campilobacterota* (*Sulfurovum*, *Desulfurella*) and the genus *Thiobacillus* are unique in the active community of the sulfur-driven autotrophic denitrification.

The permuspliner function of the splinectomeR package was used to determine significant differences between the total and active communities of both reactors over the course of the trial. The 9 most abundant genera were considered. In PR, the temporal profiles of 9 genera differed significantly in their abundances between the total and active community. In SR, 9 genera were found to differ significantly as well (Fig. S5).

3.3.3. Stochastic versus deterministic assembly processes

Microbial community assembly processes were assessed using NST analysis (Fig. S6). In the first two time points of the PR total community, stochastic processes dominated, followed by a sudden change to more deterministic influences from

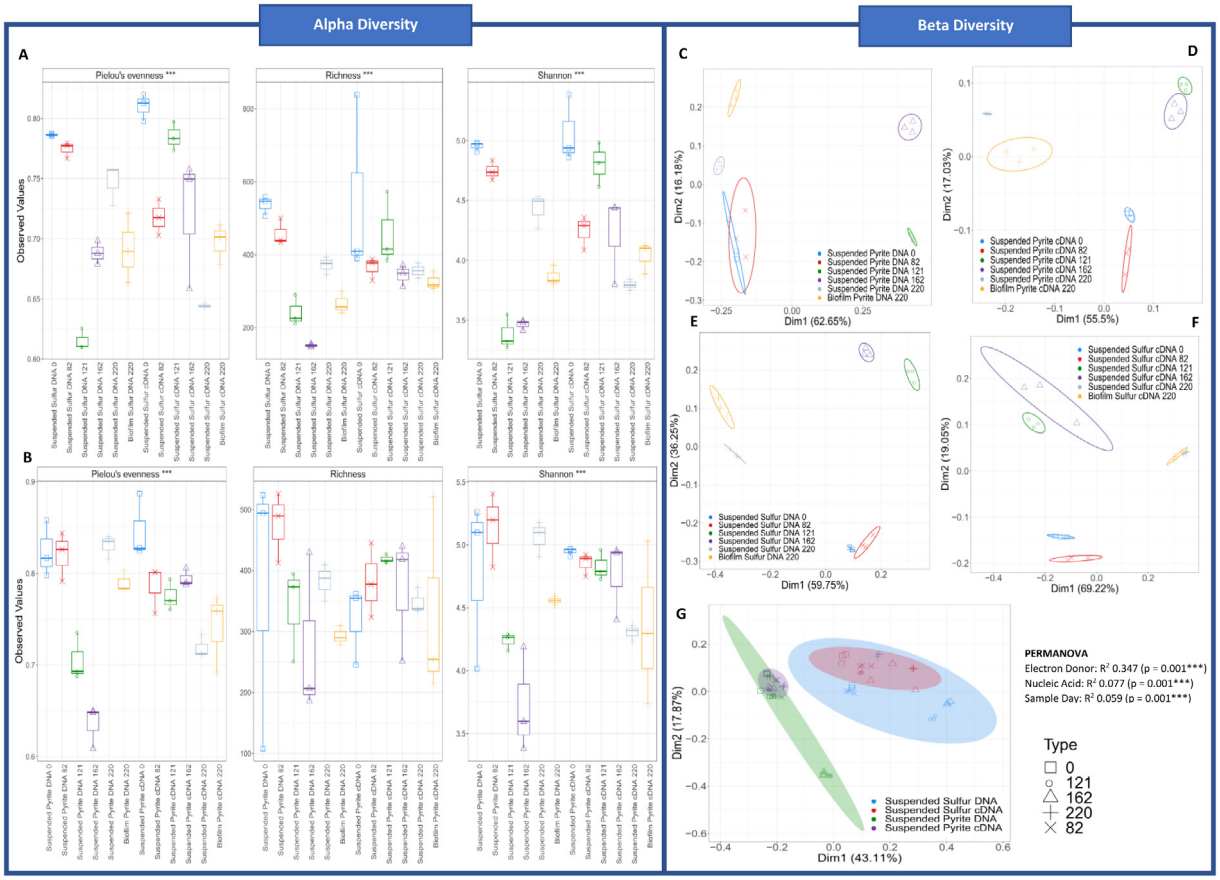

Fig. 3. Microbial community diversity. Alpha diversity indices; Rarefied Richness, Shannon Entropy and Pielou's Evenness for the total and active communities of SR (A) and PR (B). Principle Component Analysis (PCoA) of total (DNA) and active (cDNA) communities in Pyrite (C & D) and Sulfur (E & F) reactors. PCoA of all samples, grouped by electron donor (G).

day 121 (Fig. S6). The role of stochastic processes continued to decrease for the rest of the trial. Less fluctuations were observed in the active community except for the biofilm samples on day 220 which had higher levels of stochasticity (Fig. S6). The total community of SR followed the same pattern as PR. After the first two time points, a drop in the NST was detected and from days 121–220 the community was more influenced by deterministic than stochastic processes (Fig. S6).

4. Discussion

4.1. Denitrification performances of the FBRs

4.1.1. Pyrite as electron donor

This study shows that pyrite-driven autotrophic denitrification can reach denitrification rates as high as 142.4 mg $N\text{-}NO_3^-$/L·d (Table 2) in FBRs. This is, to the best of our knowledge, the maximum reported denitrification rate (Table 3) achieved with pyrite as an electron donor. The higher activity in this study can be explained using a previously enriched culture (Carboni et al., 2021), which was pre-adapted to using pyrite as substrate. Contrastingly, in the other studies, the enrichment was conducted with thiosulfate as electron donor, which is highly soluble in water and thus much more available for microbial activity (Li et al., 2016; Yang et al., 2018). In the present study, despite changes in the active microbial community (Fig. S4) from day 0 onwards, the inoculum was already pre-adapted, therefore high denitrification rates were rapidly achieved. In previous studies, pyrite-driven autotrophic denitrification has always been performed in PBRs or in batch bioassays (Li et al., 2016; Pu et al., 2015; Torrentó et al., 2010). However, the FBR configuration has several advantages such as high contact between biomass and substrate and higher substrate solubilization than packed bed reactors (Di Capua et al., 2015). Moreover, the small particle size (0.15–0.48 cm diameter) together with the fluidization may have improved mass transfer through the biofilm. Therefore, the present study demonstrates the effectiveness of FBRs for autotrophic denitrification.

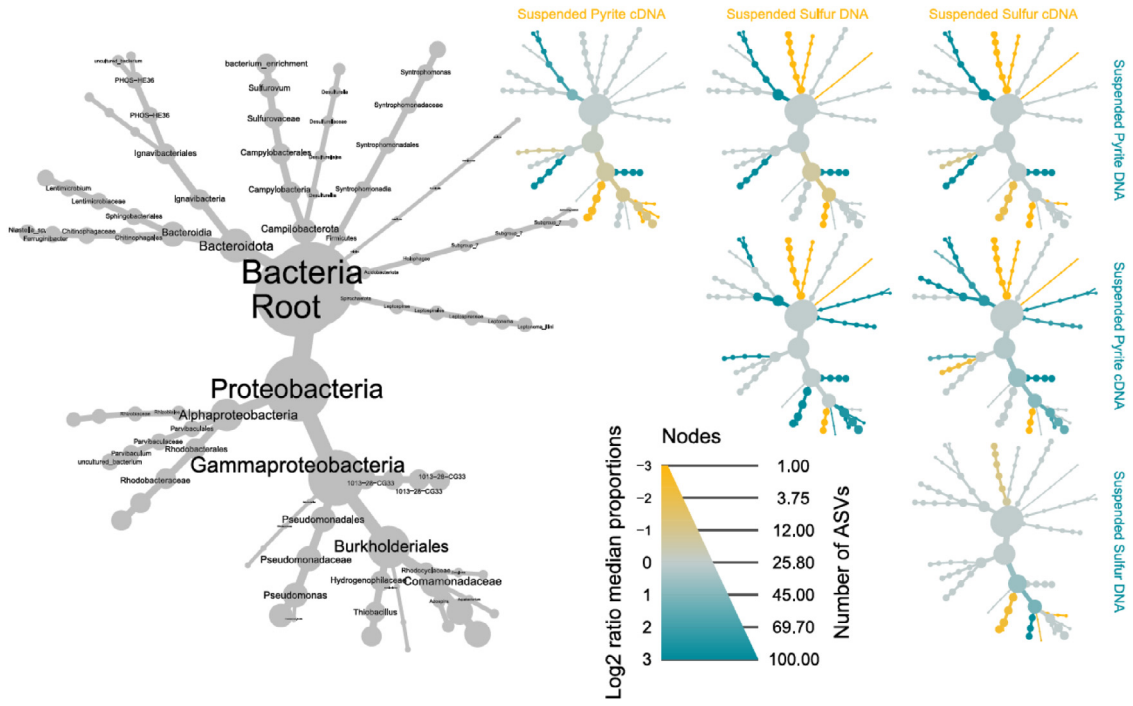

Fig. 4. Reference tree (grey) and differential heat trees with the colored branches comparing the relative abundance of the 100 most abundant ASVs (using Wilcoxin *p*-value test) between different sample groups. The circle size and the color intensity reflect the species abundance and the log2 median proportion between the two groups respectively.. (For interpretation of the references to color in this figure legend, the reader is referred to the web version of this article.)

Table 3
Autotrophic denitrification using FeS_2 or S^0 as electron donor in continuous experiments.

Electron donor	*Reactor type*	*Inoculum*	*NLR* [mg N-NO_3^-/L d]	*Removal efficiency [%]*	*Denitrification rate* [mg N-NO_3^-/L d]	*Reference*
Pyrite	PBR	Activated sludge	80	90	72	Tong et al. (2017)
	PBR	Activated sludge + SOB culture	72 185	91 47	65.5 86.9	Di Capua et al. (2020)
	PBR	Enriched anaerobic sludge	28 56	95 75	26.6 42	Li et al. (2016)
	FBR	Enriched anaerobic sludge	134 200	90 71	120.3 142.4	This study
Elemental sulfur	PBR (pilot scale)	Activated sludge from WWTP	150	100	150	Sahinkaya et al. (2015)
	PBR	Activated sludge from WWTP	114	96	109.4	(Zeng et al., 2021)
	MBBR	Activated sludge from WWTP	225	100	225	Kostrytsia et al. (2022)
	FBR	Enriched anaerobic sludge	200	91.2	184.2	This study

During the first 82 days, PR responded well to increasing NLRs, with removal efficiencies above 94% (Table 2). During this period the active and total community did not change substantially (Fig. 3), once again indicating that the pre-adapted biomass was well suited to the prevailing conditions at the beginning of the experiment. However, the high increase of the NO_3^- concentration in phase VI (from 45 to 135 mg N-NO_3^-/L) and the concomitant increase in the NLR (from 90 to 132 mg N-NO_3^-/L·d) was detrimental for the reactor performance. The microbial community during this phase did not achieve the nitrate removal efficiencies observed in the previous phases, which decreased to 69%.

In phase VII and VIII, the strategy to decrease the influent concentration to 45 and then to 35 mg N-NO_3^-/L, while maintaining the same NLR (132 mg N-NO_3^-/L·d), showed that the process of pyrite-based autotrophic denitrification needs small and progressive changes to get used to new conditions. In phase VIII, the nitrate removal efficiency reverted to 90% with a corresponding denitrification rate of 120 mg N-NO_3^-/L·d (higher than SR). Incremental changes may have been

beneficial to the microbial community, which could then progressively adapt to the new status (Fig. 3B). Di Capua et al. (2020) reported similar behavior following a 2.5-fold increase of the NLR, from 72 to 185 mg N-NO_3^-/L d, where the nitrogen removal efficiency decreased from 91% to 47%.

The high TOC concentration observed in the pyrite reactor (between 170 and 280 mg/L) during phase II, was most likely related to yeast extract in the mineral medium. Yeast extract was included as it was used in the medium in the original enrichment experiments (Carboni et al., 2021) but it was removed from the media from day 43 onward. It is possible that the yeast extract facilitated heterotrophic denitrification, since the TOC decrease in phase III corresponded with a drop in pH to 5.5 on day 43, perhaps because of acids produced during the organic carbon oxidation. The possible heterotrophic contribution to the pyrite autotrophic denitrification was not considered relevant since from phase III on, when the yeast extract was not supplied anymore, the denitrification efficiency did not decrease.

4.1.2. Elemental sulfur as electron donor

SR was a more robust configuration for autotrophic denitrification at high nitrate concentrations, treating up to 600 mg NO_3^-/L. It achieved high denitrification rates with a volumetric NO_3^- removal of 184.2 mg N-NO_3^-/L·d and stable nitrate removal efficiency between 85% and 100% (except in phase IX-A) for 220 days (Table 2). The denitrification rate obtained in this study was of the same order of magnitude compared to previous studies using sulfur as an electron donor in continuous reactors (Table 3). Sahinkaya et al. (2015) achieved a nitrogen removal rate of 150 mg N-NO_3^-/L·d from the effluent of an activatedsludgetank where the nitrate was externally supplemented at a concentration of 30–60 mg N-NO_3^-/L. Kostrytsia et al. (2022) obtained a denitrification rate of 225 mg N-NO_3^-/L·d in a moving bed-biofilm reactor system from a synthetic wastewater.

The lowest denitrification activity obtained during the 220 days FBR run was during phase IX-A when the nitrate removal efficiency decreased to 61.7% (± 11.3%). On day 186, 25 g of sulfur particles were added to the system and in phase IX-B, the nitrate removal efficiency increased to 91.2% (± 6.3%). This requirement for additional substrate is surprising, as sulfur was provided in excess already at the beginning of the trial. It is likely that the formation and precipitation of other minerals (e.g. $CaSO_4$ – Section 4.2) acted as a physical barrier and limited electron transfer (Chazal et al., 2020). The period IX-A is the only one in which the N-NO_3^- concentration in SR effluent exceeded the Usepa (2020) drinking water regulations (10 mg N-NO_3^-/L). In this phase, the maximum detected concentration was 18.48 mg N-NO_3^-/L on day 182. As a consequence of this, it is possible that sulfur-driven autotrophic denitrification requires regular maintenance, to remove the mineralized sludge. According to the present study, for such system, a maintenance frequency of 5 months would be necessary to curtail possible secondary effects on the denitrification performance.

4.2. Sulfur fate and by-products in the FBRs

The low sulfate production compared with the stoichiometric values is a phenomenon observed as well in previous studies for both pyrite and sulfur-driven autotrophic denitrification (Carboni et al., 2021; Li et al., 2016; Tong et al., 2017). Low by-product production during the denitrification process could be due to the biological or chemical processes outlined below.

In PR incomplete sulfide oxidation and resultant accumulation of extracellular S^0 storage products may have happened (Berg et al., 2014; Zhang et al., 2015). Chemical precipitation could also have occurred, since any Fe^{3+} produced during denitrification should bind with hydroxides, precipitating as $Fe(OH)_3$. This was confirmed in our study since no total Fe or Fe^{2+} was detected in solution and iron hydroxide minerals were found in the solid analysis. However, the system was never completely anaerobic since a low concentration of oxygen was found in the gas phase (data not shown). This oxygen may have contributed to pyrite oxidation and Fe^{3+} generation. If Fe^{3+} was present in excess it could have bound with sulfate present in the liquid phase, precipitating as iron sulfates as confirmed by the solid analysis (Fig. S3) and in previous studies (Carboni et al., 2021; Di Capua et al., 2020). The fixed solids (solids remaining after 2 h at 550 °C) collected on day 220 included pyrite and ferric sulfates (Table S2) which do not volatilize at 550 °C (Lychagin et al., 2019). The biomass concentration at the end of the reactor run was calculated according to the stoichiometrical reaction for pyrite-driven denitrification proposed by Tong et al. (2017) that reported a biomass growth yield of 0.085 g VSS/g N-NO_3^-. The sum of biomass and fixed solids correspond to the 82% of the total amount of solids recovered. The missing part (18% of TS) included compounds such as $Fe(OH)_3$ (9.11 g calculated from Eq. (1), corresponding to the 9% of TS) and most likely other possible precipitated minerals found in the solid sample analysis, i.e. ammonium sulfates that have a volatilization temperature lower than 550 °C (Jariwala et al., 2007).

In SR, the sulfate concentration was higher than in PR but always below the stoichiometrical value (Table S1). The fixed solids included $CaCO_3$ and other precipitated compounds such sodium and calcium sulfates that do not volatilize at 550 °C, and have melting points of 884 °C and 1450 °C, respectively (Sevonius et al., 2019; Shuai et al., 2015). In contrast, sulfur has a melting point of 115 °C and a vaporization point of 444 °C and consequentially, is not present in the measured fixed solids (Sajib and Adhikari, 2020; Zhou and Wang, 2020). The biomass growth yield for the autotrophic denitrification process using S^0 as electron donor was previously reported as 0.7 g VSS/g N-NO_3^- (Di Capua et al., 2019). The sum of the biomass and the fixed solids was 33.05 g, which corresponded to just 34.5% of TS. Therefore, the remainder (65% of TS) may have not only included minerals such ammonium sulfates (like in PR), but also the S^0 that was not used during the denitrification process.

4.3. Microbial community

4.3.1. Diversity

Beta diversity analysis indicated that there were three distinct stages of microbial community succession in both FBRs (Fig. 3C–F), potentially caused by the changes in the influent NO_3^- concentration in period VI (days 82–121). These stages aligned to changes in reactor performance: (i) beta diversity values on days 0 and 82, clustered together and corresponded with stable reactor performance; (ii) days 121 and 162 corresponded with elevated NO_3^- concentration in the influent, and (iii) day 220 which corresponded to the period after elevated NO_3^- concentration. In the 3rd stage, the microbial community was distinct from any other time point corresponding to the highest nitrate removal rates (Fig. 3C–F). This indicates that a novel microbial community may have formed as a response to the high influent NO_3^- concentration which had superior denitrification efficiency to the starting community.

The active community clustered within the total community in both FBRs (Fig. 3G), indicating that many inactive bacteria were present in the reactor biomass. Significant drops in all alpha diversity indices were observed in the total communities of both reactors following the application of high influent NO_3^- concentrations (days 121 and 162), followed by a subsequent recovery to previous levels when lowering the nitrate concentration (Phases VII–IX). In contrast, alpha diversity in the active community decreased linearly throughout the trial in both reactors indicating the evolution of a highly specialized active microbial community in both cases.

In the total community, patterns of community assembly mirrored those of the alpha diversity analysis. Initially (days 0 and 82) the total communities in both reactors had their highest NST values, indicating that stochastic processes dominated or were at least equal to deterministic processes (Fig. S6). This may be due to the pre-enrichment of the biomass under similar conditions (Carboni et al., 2021), which meant that little adaptation of the microbial community to the new environmental conditions was required. Subsequently, after the period with high influent NO_3^- concentration deterministic processes dominated and caused the total microbial community to adapt. Therefore, deterministic community assembly processes, following a sharp increase in the NO_3^- concentration, reduced the diversity, richness and evenness of both microbial communities (Fig. 3).

4.3.2. SR versus PR microbial communities

The microbial communities of SR and PR clustered separately in PCoA (Fig. 3), indicating that they were different in composition. Known sulfur oxidizers *Sulfurovum*, *Thiobacillus* and *Desulfurella* sp. were significantly more abundant in SR, whereas *Lentimicrobium sp.* and the unclassified genera *PHOS-HE36 sp. and 1013-28-CG33 sp.* were more abundant in the total community of PR (Fig. 4). The genus 1013-28-CG33 was not classified at any level, indicating it comprises understudied taxa which may contributed to autotrophic denitrification. *PHOS-HE36* sp. from the *Ignavibacteriales* order is reasonably common in autotrophic denitrification systems (Kostrytsia et al., 2018). It was detected in the previous enrichment experiment which was used as inoculum for the present study (Carboni et al., 2021). Microorganisms belonging to *Ignavibacteriales* can perform nitrate reduction from NO_3^- to N_2O using *napA, nirK,* and *norB* genes. The *nosZ* gene catalyzes the reduction of N_2O to N_2 and is present in the genome of *I. Album* (Bei et al., 2021). *Lentimcrobium, Pseudomonas* and *Comamonadaceae* sp. were significantly more abundant in the active community of PR than SR, whereas *Parvibaculum sp.* were more abundant in the active community of SR than PR.

4.3.2.1. Pyrite reactor. *Lentimicrobium* sp. were the most abundant taxa in the total community of PR in the first two timepoints. Subsequently, on day 121, after the high influent NO_3^- concentration, *1013-28-CG33 sp.* and *PHOS-HE36 sp.* became dominant in the total community (Fig. S4 & Fig. S5). However, their abundance did not increase in the active community, perhaps indicating that their increase in RA was caused by a decrease in the presence of other taxa. *Pseudomonas* sp. were much more abundant in the active community of PR (Fig. 4), particularly prior to the concentration change (days 0 and 82) (Fig. S4 & Fig. S5). However, their abundance decreased after the influent NO_3^- concentration change on day 82, indicating that they may have a key role in denitrification but at lower nitrate concentrations. Subsequently, their abundance did not recover to previous levels, and the prevalence of other taxa such as *Ferruginibacter sp.* and *Rhodococcus sp.* increased (Fig. S4). Both of these taxa are able to perform autotrophic denitrification (Kostrytsia et al., 2018; Pang and Wang, 2020) and based on this evidence may be more competitive at higher nitrate levels. On day 220 the active microbial community had low diversity mainly as consequences of decreased evenness (Fig. 3), potentially due to the progressive specialization of the community over time.

4.3.2.2. Elemental sulfur reactor. *Thiobacillus sp.* and *Sulfurovum sp.* dominated the total microbial community of SR during the 220 days of the reactor run (Fig. S4). *Thiobacillus sp.* are known to exploit reduced sulfur compounds as electron donors (Huang et al., 2020; Chazal et al., 2020; Zhang et al., 2022) and *Sulfurovum sp.* are also frequently found in autotrophic denitrification literature (Li et al., 2022; Xu et al., 2016). The temporal patterns of *Thiobacillus* and *Sulfurovum sp.* relative abundance were inversely related throughout the course of the trial (Fig. S5) in both the active and total communities. It is clear that *Thiobacillus* sp. were more abundant during the perturbed phase of reactor operation (days 121 and 162) (Fig. S5), but were much less prominent during stable periods, particularly in the active community when *Sulfurovum sp.* were more dominant. The ability of *Thiobacillus sp.* to proliferate during this period of instability may be what allowed SR to recover better than PR upon changing the influent NO_3^- concentration (Fig. 1). *Pseudomonas sp.* were also significantly more abundant in the active community in SR (Fig. 4) but decreased as the NLR was increased, once again indicating their role in autotrophic denitrification at lower nitrate concentrations.

4.3.3. Functional redundancy drives process recovery

The differences in composition of the total and active microbial communities and the establishment of alternative organisms after the NO_3^- concentration change (e.g. *Ferruginibacter sp.* and *Rhodococcus sp.* in PR and *Thiobacillus sp.* in SR) indicate that there may have been some functional redundancy in the initial communities which helped both systems to respond to increased NLR. Functional redundancy has previously been suggested to impart more stability and resilience to microbial communities (Botton et al., 2006; Louca et al., 2018) and therefore help to preserve functions in environmental biotechnologies experiencing perturbations. This is assumed to be because of the presence of multiple organisms which can perform the same function (Vanwonterghem et al., 2016; Wittebolle et al., 2008) and could therefore respond to environmental perturbations. This may have been the case in the current study, where *Ferruginibacter sp.* and *Rhodococcus sp.* became more important for PR after the high influent NO_3^- concentration in phase VI and *Thiobacillus sp.* were more active in SR. Therefore, the current study demonstrates the importance of functional redundancy for dealing with sudden increases of nitrate concentration in autotrophic denitrification.

5. Conclusions

Denitrification with pyrite as the electron donor was successful up to NLRs as high as 200 mg $N\text{-}NO_3^-$/L·d. Pyrite based denitrification has several advantages for the autotrophic denitrification process. The pH during the bioconversion is constant, therefore no buffer is required, making it more cost effective than sulfur-driven denitrification which requires the addition of buffering compounds such as $CaCO_3$. In addition, $CaCO_3$ and SO_4^{2-} production from S^0 oxidation results in the precipitation of calcium sulfates which need to be removed from the reactor at a frequency of approximately 5 months. In pyrite-based denitrification, sulfate concentrations in the effluent were always below 4.13% of the theoretical expected concentration. Three distinct stages of microbial community succession were observed in both reactors before, during and after a period of feeding medium with high nitrate (135 mg $N\text{-}NO_3^-$/L) concentrations (Phase VI). Alpha diversity of the total microbial community decreased significantly after the concentration change in both SR and PR, but recovered to previous levels after process stabilization. The active community, however, demonstrated a linear decrease in alpha diversity, indicating the evolution of a highly specialized microbial community. Both systems recovered after the nitrate increase during phase VI, possibly due to high degrees of functional redundancy in the microbial community. In SR *Thiobacillus sp.* were more abundant after phase VI, whereas *Sulfurovum sp.* were more abundant during steady reactor operation. This indicates that *Thiobacillus sp.* may have enabled SR to recover from the high NO_3^- concentrations more quickly than PR. High NLRs (> 142.4 mg $N\text{-}NO_3^-$/L·d) resulted in incomplete denitrification in PR, whereas complete denitrification was achieved in SR up to 184.4 mg $N\text{-}NO_3^-$/L·d.

CRediT authorship contribution statement

Maria F. Carboni: Conceptualization, Data curation, Investigation, Formal analysis, Writing – original draft, Writing – review & editing, Visualization. **Simon Mills:** Conceptualization, Methodology, Data formal analysis, Visualization, Supervision, Writing – review & editing. **Sonia Arriaga:** Conceptualization, Supervision, Writing – review & editing. **Gavin Collins:** Supervision, Writing – review & editing. **Umer Z. Ijaz:** Data formal analysis, Visualization, Writing – review & editing. **Piet N.L. Lens:** Supervision, Project administration, Writing – review & editing, Funding acquisition.

Declaration of competing interest

The authors declare that they have no known competing financial interests or personal relationships that could have appeared to influence the work reported in this paper.

Data availability

Data will be made available on request.

Acknowledgments

The authors thank Borja Khatabi Soliman Tamayo and Leah Egan (NUIG, Ireland) for their help and support during the laboratory work, Manuel Suarez (NUIG, Ireland) for assisting in reactor operation and Carlos Sanchez (NUI Galway) for drawing the reactor scheme (Fig. S1). All authors contributed to the article and approved the submitted version.

Funding source

This publication has emanated from research supported by Science Foundation Ireland (SFI) through the SFI Research Professorship Programme entitled *Innovative Energy Technologies for Biofuels, Bioenergy and a Sustainable Irish Bioeconomy* (IETSBIO^3; grant number 15/RP/2763) and the Research Infrastructure research, Ireland grant *Platform for Biofuel Analysis* (Grant Number 16/RI/3401). GC and SM were supported by a European Research Council Starting Grant (3C-BIOTECH 261330) and by a Science Foundation Ireland Career Development Award, Ireland (17/CDA/4658), awarded to GC. UZI is further supported by a NERC Independent Research Fellowship, Ireland (NE/L011956/1) and EPSRC, United Kingdom (EP/P029329/1 and EP/V030515/1).

Appendix A. Supplementary data

Supplementary material related to this article can be found online at https://doi.org/10.1016/j.eti.2022.102878.

References

APHA, 2012. Standard Methods for Examination of Water and Wastewater 2012. American Public Health Association, Washington, DC.

Bei, Qicheng, Peng, Jingjing, Liesack, Werner, 2021. Shedding light on the functional role of the Ignavibacteria in Italian rice field soil: A meta-genomic/transcriptomic analysis. Soil Biol. Biochem. 163 (May), 108444.

Berg, Jasmine S., Schwedt, Anne, Kreutzmann, Anne Christin, Kuypers, Marcel M.M., Milucka, Jana, 2014. Polysulfides as intermediates in the oxidation of sulfide to sulfate by Beggiatoa spp. Appl. Environ. Microbiol. 80 (2), 629–636.

Botton, S., van Heusden, M., Parsons, J.R., Smidt, H., van Straalen, N., 2006. Resilience of microbial systems towards disturbances. Crit. Rev. Microbiol. http://dx.doi.org/10.1080/10408410600709933.

Carboni, M.F., Florentino, A.P., Costa, R.B., Zhan, X., Lens, P.N.L., 2021. Enrichment of autotrophic denitrifiers from anaerobic sludge using sulfurous electron donors. Front. Microbiol. 12, 678323. http://dx.doi.org/10.3389/fmicb.2021.678323.

Chazal, M.P., Carboni, Maria F., Lens, Piet N.L., 2020. Interactions of the sulfur and nitrogen cycles: microbiology and process technology. In: Environmental Technologies to Treat Sulfur Pollution: Principles and Engineering, Piet N. L. Lens. IWA Publishing, pp. 403–443. http://dx.doi.org/10.2166/9781789060966.

Cline, J.D., 1969. Spectrophotometric determination of hydrogen sulfide in natural waters. Limnol. Oceanogr. 14, 454–458. http://dx.doi.org/10.4319/lo.1969.14.3.0454.

Costa, R.B., Bevilaqua, D., Lens, P. N.L., 2020. Pre-treatment and temperature effects on the use of slow release electron donor for biological sulfate reduction. J. Environ. Manag. 275, 111216. http://dx.doi.org/10.1016/j.jenvman.2020.111216.

Di Capua, Francesco, Mascolo, Maria Cristina, Pirozzi, Francesco, Esposito, Giovanni, 2020. Simultaneous denitrification, phosphorus recovery and low sulfate production in a recirculated pyrite-packed biofilter (RPPB). Chemosphere 255, 126977.

Di Capua, Francesco, Papirio, Stefano, Lens, Piet N.L., Esposito, Giovanni, 2015. Chemolithotrophic denitrification in biofilm reactors. Chem. Eng. J. 280, 643–657.

Di Capua, F., Pirrozzi, F., Lens, P.N.L., Esposito, G., 2019. Electron donors for autotrophic denitrification. Chem. Eng. J. http://dx.doi.org/10.1016/j.cej.2019.01.069.

Fernández-Nava, Marañón, Soons, Castrillon, 2010. Denitrification of high nitrate concentration wastewater using alternative carbon sources. J. Hazard. Mater. http://dx.doi.org/10.1016/j.jhazmat.2009.08.140.

Florentino, Anna Patrícya, Costa, Rachel Biancalana, Hu, Yuansheng, Flaherty, Vincent O., Lens, Piet N.L., 2020. Long chain fatty acid degradation coupled to biological sulfidogenesis: A prospect for enhanced metal recovery. Front. Bioeng. Biotechnol. 8 (October), 1–14.

Griffiths, R.I., Whiteley, A.S., O'Donnell, A.G., Bailey, M.J., 2000. Rapid method for coextraction of DNA and RNA from natural environments for analysis of ribosomal DNA- and rRNA-based microbial community composition. Appl. Environ. Microbiol. http://dx.doi.org/10.1128/AEM.66.12.5488-5491.2000.

Hu, Yuansheng, Wu, Guangxue, Li, Ruihua, Xiao, Liwen, Zhan, Xinmin, 2020. Iron sulphides mediated autotrophic denitrification: An emerging bioprocess for nitrate pollution mitigation and sustainable wastewater treatment. Water Res. 179, 115914.

Huang, Cong, Liu, Qian, Chen, Xueqi, Nan, Jun, Li, Zhiling, Wang, Aijie, 2020. Bioaugmentation with *Thiobacillus* sp. H1 in an autotrophic denitrification desulfurization microbial reactor: Microbial community changes and relationship. Environ. Res. 189, http://dx.doi.org/10.1016/j.envres.2020.109927.

Jariwala, Maheshwari, Crawford, Jessica, LeCaptain, Dale J., 2007. In situ Raman spectroscopic analysis of the regeneration of ammonium hydrogen sulfate from ammonium sulfate. Ind. Eng. Chem. Res. 46 (14), 4900–4905.

Jessen, Søren, Dieke, Postma, Lærke, Thorling, Müller, Sascha, Leskelä, Jari, Engesgaard, Peter, 2017. Decadal variations in groundwater quality: A legacy from nitrate leaching and denitrification by pyrite in a sandy aquifer. Water Resour. Res. http://dx.doi.org/10.1002/2016WR018995.

Kadam, Somnath S., Mesbah, Ali, Windt, Eric Van Der, Kramer, Herman J.M., 2010. Chemical engineering research and design rapid online calibration for ATR-FTIR spectroscopy during batch crystallization of ammonium sulphate in a semi-industrial scale crystallizer. Chem. Eng. Res. Des. 89 (7), 995–1005.

Khanongnuch, Ramita, Capua, Francesco Di, Lakaniemi, Aino Maija, Rene, Eldon R., Lens, Piet N.L., 2019. Transient–state operation of an anoxic Biotrickling filter for H2S removal. J. Hard Mater. 377 (3), 42–51.

Kiefer, Johannes, Stark, Alexander, Kiefer, Agnita Lynda, Heike, Glade, 2018. Infrared spectroscopic analysis of the inorganic deposits from water in domestic and technical heat exchangers. mpdi energies http://dx.doi.org/10.3390/en11040798.

Kostrytsia, Anastasiia, Papirio, Stefano, Khodzhaev, Murod, Morrison, Liam, Collins, Gavin, Lens, Piet N.L., Ijaz, Umer Zeeshan, Esposito, Giovanni, 2022. Biofilm carrier type affects biogenic sulfur-driven denitrification performance and microbial community dynamics in moving-bed biofilm reactors. Chemosphere 287 (P1), 131975.

Kostrytsia, Anastasiia, Papirio, Stefano, Morrison, Liam, Ijaz, Umer Zeeshan, Collins, Gavin, Lens, Piet N.L., Esposito, Giovanni, 2018. Biokinetics of microbial consortia using biogenic sulfur as a novel electron donor for sustainable denitrification. Bioresour. Technol. 270 (August), 359–367.

Li, Ruihua, Morrison, Liam, Collins, Gavin, Li, Aimin, Zhan, Xinmin, 2016. Simultaneous nitrate and phosphate removal from wastewater lacking organic matter through microbial oxidation of pyrrhotite coupled to nitrate reduction. Water Res. 96, 32–41.

Li, Yingying, Wang, Yali, Wan, Dongjin, Li, Bang, Zhang, Panyue, Wang, Hongjie, 2020. Bioresource technology pilot-scale application of sulfur-limestone autotrophic denitri Fi cation bio Fi lter for municipal tailwater treatment Performance and microbial community structure 300(october 2019).

Li, Wei, Zhen, Yuming, Li, Nan, Wang, Hengqi, Lin, Minghui, Guo, Ping, Lin, Jianguo, 2022. Sulfur transformation and bacterial community dynamics in both desulfurization-denitrification biofilm and suspended activated sludge. Bioresour. Technol. http://dx.doi.org/10.1016/j.biortech.2021.126108.

Liao, Runhua, Shen, Ke, Li, Ai-min, Shi, Peng, Li, Yan, Shi, Qianqian, Wang, Zhu, 2013. Bioresource technology high-nitrate wastewater treatment in an expanded granular sludge bed reactor and microbial diversity using 454 pyrosequencing analysis. Bioresour. Technol. 134, 190–197.

Liu, T., Hu, Y., Chen, N., He, Q., Feng, C., 2021. High redox potential promotes oxidation of pyrite under neutral conditions: Implications for optimizing pyrite autotrophic denitrification. J. Hard Mater. 416, 125844.

Louca, Stilianos, Polz, Martin, Mazel, Florent, Albright, Michaeline, Huber, Julie, O'Connor, Mary, Ackermann, Martin, Hahn, Aria, Srivastava, Diane, Crowe, Sean, Doebely, Michael, Parfrey, Laura, 2018. Function and functional redundancy in microbial systems. Nat. Ecol. Evol..

Lu, Hui, Ekama, George A., Wu, Di, Feng, Jiang, Van Loosdrecht, Mark C.M., Chen, Guang-hao, 2011. SANI process realizes sustainable saline sewage treatment : Steady state model-based evaluation of the pilot-scale trial of the process total nitrogen. 6.

Lychagin, D.V., Bibko, A.A., Zyryanova, L.A., 2019. Features of plastic deformations of quartz-pyrite-mineral associations of the gabriel mine. AIP Conf. Proc. 2167 (November).

Majzlan, Juraj, Alpers, Charles N., Bender, Christian, Mccleskey, R. Blaine, Myneni, Satish C.B., Neil, John M., 2011. Vibrational, X-ray absorption, and Mössbauer spectra of sulfate minerals from the weathered massive sulfide deposit at iron mountain, California. Chem. Geol. 284 (3–4), 296–305.
Mills, S., Trego, A.C., Lens, P.N.L., Ijaz, U.Z., Collins, G., 2021. A distinct, flocculent, acidogenic microbial community accompanies methanogenic granules in anaerobic digesters. Microbiol. Spectrum 9 (3).
Ogbughalu, Omy T., Vasileiadis, Sotirios, Schumann, Russell C., Gerson, Andrea R., Li, Jun, St, Roger, Smart, C., Short, Michael D., 2020. Role of microbial diversity for sustainable pyrite oxidation control in acid and metalliferous drainage prevention. J. Hard Mater. 393 (February), 122338.
Pang, Yunmeng, Wang, Jianlong, 2020. Insight into the mechanism of chemoautotrophic denitrification using pyrite (FeS_2) as electron donor. Bioresour. Technol. 318 (July), 124105.
Parada, Alma E., Needham, David M., Fuhrman, Jed A., 2016. Every base matters: Assessing small subunit RRNA primers for marine microbiomes with mock communities. In: Time Series and Global Field Samples, vol. 18, pp. 1403–1414.
Pu, Jiaoyang, Feng, Chuanping, Liu, Ying, Li, Rui, Kong, Zhe, Chen, Nan, Tong, Shuang, Hao, Chunbo, Liu, Ye, 2015. Pyrite-based autotrophic denitrification for remediation of nitrate contaminated groundwater. Bioresour. Technol. 173, 117–123.
Rezania, B., Oleszkiewicz, J.A., Cicek, N, Mo, H., 2005. Hydrogen-dependent denitrification in an alternating anoxic-aerobic SBR membrane bioreactor. Water Sci. Technol. 51 (6–7), 403–409.
Sahinkaya, Erkan, Kilic, Adem, Duygulu, Bahadir, 2014. Sciencedirect pilot and full scale applications of sulfur-based autotrophic denitrification process for nitrate removal from activated sludge process effluent. Water Res. 60, 210–217.
Sahinkaya, Erkan, Yurtsever, Adem, Aktaş, Özgür, Ucar, Deniz, Wang, Zhiwei, 2015. Sulfur-based autotrophic denitrification of drinking water using a membrane bioreactor. Chem. Eng. J. 268, 180–186.
Sajib, S.K., Adhikari, S., 2020. Effect of pyrolysis method on physical properties of activated biochar and its application as cathode material for lithium-sulfur battery. Am. Soc. Agric. Biol. Eng. 63 (2), 485–493.
Sevonius, Christoffer, Yrjas, Patrik, Lindberg, Daniel, Hupa, Leena, 2019. Impact of sodium salts on agglomeration in a laboratory fluidized bed. Fuel 245 (February), 305–315.
Shuai, Cijun, Zhou, Jianhua, Wu, Ping, Gao, Chengde, Feng, Pei, Xiao, Tao, Deng, Youwen, Peng, Shuping, 2015. Enhanced stability of calcium sulfate scaffolds with 45S5 bioglass for bone repair. Materials 8 (11), 7498–7510.
Stams, A.J.M., Van Dijk, J.B., Dijkema, C., Plugge, C.M., 1993. Growth of syntrophic propionate-oxidizing bacteria with fumarate in the absence of methanogenic bacteria. Appl. Environ. Microbiol. 59 (4), 1114–1119.
Tong, Shuang, Rodriguez-gonzalez, Laura C., Feng, Chuanping, Ergas, Sarina J., 2017. Comparison of particulate pyrite autotrophic denitrification (PPAD) and sulfur oxidizing denitrification (SOD) for treatment of nitrified wastewater. pp. 239–246.
Torrentó, Clara, Cama, Jordi, Urmeneta, Jordi, Otero, Neus, Soler, Albert, 2010. Denitrification of groundwater with pyrite and Thiobacillus denitrificans. Chem. Geol. 278 (1–2), 80–91.
Trego, A.C., McAteer, P.G., Nzeteu, C., Mahony, T., Abram, F., Ijaz, U.Z., O'Flaherty, V., 2021. Combined stochastic and deterministic processes drive community assembly of anaerobic microbiomes during granule flotation. Front. Microbiol. 12, 1165.
Ucar, Deniz, Yilmaz, Tulay, Di Capua, Francesco, Esposito, Giovanni, Sahinkaya, Erkan, 2020. Comparison of biogenic and chemical sulfur as electron donors for autotrophic denitrification in sulfur-fed membrane bioreactor (SMBR). Bioresour. Technol. 299 (October 2019), 122574.
Usepa, 2020. National drinking water regulations. https://www.epa.gov/sdwa.
Vanwonterghem, Inka, Jensen, Paul, Rabaey, Korneel, Tyson, Gene, 2016. Genome-centric resolution of microbial diversity, metabolism and interactions in anaerobic digestion. Environ. Microbiol. http://dx.doi.org/10.1111/1462-2920.13382.
Vasiliadou, I.A., Karanasios, K.A., Pavlou, S., D.V., Vayenas., 2009. Experimental and modelling study of drinking water hydrogenotrophic denitrification in packed-bed reactors 165. pp. 812–824.
Wang, Hui-long, Cui, Jin-yan, Jiang, Wen-feng, 2011. Synthesis, characterization and flocculation activity of novel $Fe(OH)_3$ – Polyacrylamide hybrid polymer. Mater. Chem. Phys. 130 (3), 993–999.
Wittebolle, Lieven, Vervaeren, Han, Verstraete, Willy, Nico, Boon, 2008. Quantifying community dynamics of nitrifiers in functionally stable reactors. Appl. Environ. Microbiol. http://dx.doi.org/10.1128/AEM.01006-07.
Xu, Jinlan, Fan, Yimin, Li, Zhixu, 2016. Effect of pH on elemental sulfur conversion and microbial communities by autotrophic simultaneous desulfurization and denitrification. Environ. Technol. http://dx.doi.org/10.1080/09593330.2016.1173117.
Yang, Yan, Gerrity, Sean, Collins, Gavin, Chen, Tianhu, Li, Ruihua, Xie, Sihuang, 2018. Enrichment and characterization of autotrophic Thiobacillus denitrifiers from anaerobic sludge for nitrate removal. Process Biochem. 68 (December 2017), 165–170.
Zhang, Ruo-Chen, Chen, Chuan, Xu, Xi-Jun, Lee, Duu-Jong, Ren, Nan-Qi, 2022. The interaction between *pseudomonas c27* and *thiobacillus denitrificans* in the integrated autotrophic and heterotrophic denitrification process. Sci. Total Environ. 811, http://dx.doi.org/10.1016/j.scitotenv.2021.152360.
Zhang, Muzi, Yin, Xiao, Li, Ming, Wang, Rixin, Qian, Yunxia, Hong, Meiling, 2020. Effect of nitrite exposure on haematological status, oxidative stress, immune response and apoptosis in yellow catfish (*Pelteobagrus fulvidraco*). Comp. Biochem. Physiol. Part C: Toxicol. Pharmacol. http://dx.doi.org/10.1016/j.cbpc.2020.108867.
Zhang, Lili, Zhang, Chao, Hu, Chengzhi, Liu, Huijuan, Qu, Jiuhui, 2015. Denitrification of groundwater using a sulfur-oxidizing autotrophic denitrifying anaerobic fluidized-bed MBR: Performance and bacterial community structure. Appl. Microbiol. Biotechnol. 99 (6), 2815–2827.
Zhou, Dong, Wang, Guoxiu, 2020. Supercool sulfur. Nature Nanotechnol. 15 (3), 167–168.
Zou, G., Papirio, S., Lakaniemi, A.M., Ahoranta, S.H., Puhakka, J.A., 2016. High rate autotrophic denitrification in fluidized-bed biofilm reactors. Chem. Eng. J. 284, 1287–1294.